https://doi.org/10.5194/ar-2026-20
Preprint. Discussion started: 11 June 2026

AEROSOL Research Discussions

Look−up tables for complex refractive index correction of particle sizes measured by common research−grade optical particle counters

Paola Formenti[1] and Claudia Di Biagio[1]

[1] Université Paris Cité and Univ Paris Est Creteil, CNRS, LISA, F−75013 Paris, France

Corresponding author: Paola Formenti (paola.formenti@lisa.ipsl.fr)

Abstract

Optical particle counters (OPC) are widely used to measure the aerosol particle number size distribution over a large size range encompassing sub- and super-micron diameters. The measurement principle of OPCs is based on the dependence of light scattering on particle size. However, this dependence is not monotonic at all sizes as light scattering also depends on the particle composition (i.e., the complex refractive index, *m*) and morphology. Therefore, the conversion of the measured scattered intensity to the particle size depends on the microphysical properties of the sampled aerosol population and might not be unique at all sizes. While these complexities have been considered before, corrections are typically applied ad-hoc and are not standardised. This paper addresses this issue by providing a consistent and extended database of pre−computed correction factors for a wide range of complex refractive index values representing the composition variability of atmospheric aerosols. These correction factors are calculated for five different commercial OPCs by assuming Mie theory for homogeneous spherical particles, and by varying the real part of the complex refractive index between 1.33 and 1.75 in steps of 0.01 and the imaginary part between 0.0 and 0.4 in steps of 0.001. The datasets are distributed for data users/geophysicists using number size distribution measurements from OPC for their research on atmospheric aerosols. Application and caveats of the corrections factors are discussed, and key recommendations are provided to ensure the robustness and consistency of size distribution datasets.

1. Introduction

Aerosol particles are amongst the more elusive and at the same time climate−relevant components of the atmosphere (Szopa et al., 2021). While airborne, they interact with atmospheric radiation at wavelengths from the ultra−violet to the infrared, and act as

https://doi.org/10.5194/ar-2026-20
Preprint. Discussion started: 11 June 2026

condensation nuclei for liquid and ice clouds (Seinfeld and Pandis, 2006). Upon deposition, they can change the productivity of marine and land ecosystems (Kanakidou et al., 2018). They also affect the atmospheric composition directly by their emission, and indirectly, as a sink of some reactive gases (e.g., Seinfeld and Pandis, 2006; Kanakidou et al., 2018). Through these processes aerosol particles affect the Earth's climate but they can also impact the environment in various and severe ways. Aerosol particles can degrade air quality to the detriment of human health (Shiraiwa et al., 2017) and the conservation of cultural heritage (Bonazza et al., 2017).

These varied effects of aerosols are largely made possible by their extended size spectrum. Atmospheric aerosol particles are characterised by sizes ranging from a few nanometres to tens of micrometres depending on the source and the mechanism of emission, and on the transformation that they undergo whilst airborne (Seinfeld and Pandis, 2006). The typical particle size distribution in the atmosphere is a continuum of four lognormal modes (nucleation, comprising particles with diameters up to 10 nm; Aitken, comprising particles of diameters ranging from 10 nm to 100 nm; accumulation, made up of particles from 100 nm to approximately 2.5 μm in diameter; coarse, comprising particles of diameter larger than 2.5 μm), with different amplitude, mode diameter, relative proportions, chemical composition, and lifetimes (Seinfeld and Pandis, 2006).

Whilst the particle size distribution is a critical parameter to assess the effects of aerosols on radiation, clouds, chemistry, ocean and terrestrial productivity, and human health, its measurement is challenging. There is no instrumental technique covering the entire particle size range but only portions of it. Furthermore, these different instrumental techniques measure particle size using various operating principles, ranging from light-scattering, aerodynamic and electric mobility properties of aerosol (Baron and Willeke, 2001; Hinds, 1999). As a result, the particle size measured experimentally is an operational definition that depends on the particle density, real and complex refractive index (*m*, the property of matter relating spectral optical properties to chemical composition), and morphology (Baron and Willeke, 2001; Hinds, 1999).

Amongst these experimental techniques, optical particle counters (OPCs) provide fast (better than 1 Hz) measurements over a large dynamic range, both in concentration and size, including sub− and super−micron particles (Baron and Willeke, 2001; Hinds, 1999; Wendisch and Brenguier, 2013). The operating principle of the OPC is based on the fact that the intensity of monochromatic or white light scattered by an airborne particle (single or ensembles) in a given scattering direction depends on its size (Baron and Willeke, 2001; Hinds, 1999; Wendisch and Brenguier, 2013); as a consequence, the intensity of light−scattering measured in a known sensing volume and at known wavelength can be converted into particle size. By

https://doi.org/10.5194/ar-2026-20
Preprint. Discussion started: 11 June 2026

adapting the geometry of the sensing volume (angular range of collected scattering) and the wavelength of the light source, the design of the OPC can be customised to different applications (i.e., sampling mostly fine or coarse particles, more or less absorbing aerosols, minimise the effects of asphericity.…), therefore making them a versatile tool for atmospheric aerosol research. Research−grade OPCs are used worldwide in laboratory and field studies, in particular as a core instrument on research aircraft during a range of field campaigns (e.g., Collins et al., 2000; Haywood et al., 2003a; 2003b; Reid et al., 2003; Osborne et al., 2008; Ryder et al., 2013; Di Biagio et al., 2015; Denjean et al., 2016; Petzold et al., 2009; Weinzerl et al., 2017; De Perim de Faria et al., 2017; Schafer et al., 2019; Brock et al., 2019; Wu et al., 2020; Howell et al., 2021; Lewis et al., 2026, amongst others).

The scattering cross-section C_{sca} measured by an OPC within a certain angular range can be converted into an optical equivalent diameter (D_{OE}) based on calibration with non−absorbing spherical particle latex spheres (PSL) or equivalent scattering material of known m at the working wavelength of the instrument. However, atmospheric aerosols have different composition than the calibration material, and the intensity of scattered light also depends on particle morphology (Dubovik et al., 2006; Huang et al., 2021). The differences in m and morphology between the calibration spheres and natural aerosols cause the OPC-determined size to be different from the real size of ambient aerosol particle. The error in the particle size can propagate to size-relevant datasets, such as for example their mass absorption and scattering cross sections or single scattering albedo, ultimately generating biases in the estimates of aerosol impacts on the weather, climate, and human health (Huang et al., 2021). Henceforth, representing the number size distribution of atmospheric aerosol requires being able to convert the value of D_{OE} into an equivalent spherical particle geometrical (i.e., volume equivalent) diameter (D_{geo}) corresponding to the m of the sampled aerosols at the operating wavelength of the OPC. The D_{geo} is defined as the diameter of a sphere having the same volume as the particle under consideration. Converting D_{OE} to D_{geo} reduces the dependence of size distribution measurements on particle composition (m), thereby enabling comparison between measurements obtained under different aerosol conditions. In practice, the equivalence between D_{OE} at the reference m of the calibration material and D_{geo} at the m of the ambient aerosols is obtained by calculating, at each m value, the value of D_{geo} corresponding to the same scattering cross−section C_{sca} than that obtained when using D_{OE}. However, the scattering cross−section may not depend linearly or at least in a monotonic way on particle diameter (Bohren and Huffmann, 1983). In the approximation of spherical particles, this effect is due to the Mie resonance and ripple oscillations in the light scattering functions. As a consequence, for a given m and D_{OE}, the scattering cross−section C_{sca} might correspond to a number of values of D_{geo} and the solution might not be unique. This is a well−known and

https://doi.org/10.5194/ar-2026-20
Preprint. Discussion started: 11 June 2026

documented problem in the expert community (e.g., Garvey and Pinnick, 1983; Liu et al., 1992; Jaenicke and Hanusch, 1993; Pinnick et al., 2000; Collins et al., 2000; Reid et al., 2003; Osborne et al., 2008; Petzold et al., 2009; Rosenberg et al., 2012; Wendisch and Brenguier, 2013; Brock et al., 2016; 2019; Walser et al., 2017; Moore et al., 2021; Lewis et al., 2026). This problem is dealt by scientists in two major ways, according to their expertise:

1/ instrument developers/engineers have proposed processing methodologies taking into account the entire chain of operations, in particular the calibration both in size and intensity. Indeed, Rosenberg et al. (2012) described a mathematical method that takes into account the OPC size and pulse height calibration and a probability density function to calculate mean diameters and widths for OPC bins based upon Mie-Lorenz theory for measured aerosol particles whose scattering properties are different to those of the calibration material (e.g., Walser et al., 2017)

2/ data users/geophysicists relying on external expertise for calibration/instrument characterization and have proposed methods for adapting the measured size distribution to the ambient refractive indices, which have at times been evaluated by concurrent measurements of the aerosol composition (e.g., Di Biagio et al. 2015; 2017; Denjean et al., 2016).

Building on expert investigations, this work is addressed to environmental scientists or data analysts who make use of data from some of the most common research−grade OPCs available through open−access datasets. Such datasets are becoming more and more popular through large−scale ground−based and airborne environmental research infrastructures, notably in Europe (e.g., Aerosol, Clouds and Trace Gases, ACTRIS, https://www.actris.fr/actris−eu/; In−service Aircraft for a Global Observing System, IAGOS, www.iagos.org; and EUropean Facility for Airborne Research, EUFAR https://www.eufar.net/) and integrative science projects (eg., the Global Aerosol Synthesis and Science Project, GASSP; Reddington et al., 2017). While using the data for their research and publications, these users are not necessarily data instrument operators, nor necessarily have the knowledge, expertise or time to perform and evaluate the *m*−adapted corrections.

This paper describes the provision of standardized corrections of particle sizing in order to take into account the dependence of angular scattering on particle composition, represented by the particle complex refractive index *m*. The dataset consists of look−up tables of pre−computed scattering functions and size correction factors as downloadable ascii files, covering a range of complex refractive index values relevant to atmospheric aerosols. Calculations are performed under the hypothesis of spherical particles, which is a good approximation for a

https://doi.org/10.5194/ar-2026-20
Preprint. Discussion started: 11 June 2026

wide range of aerosol types and conditions. We present the dataset and provide with recommendations for its use.

2. Methods

2.1. Instruments

Instruments considered in this paper are common research−grade OPC used onboard aircraft and for surface measurements, including laboratory studies. They are:

1. The Passive Cavity Aerosol Spectrometer Probe (PCASP, Model 100X, Droplet Measurement Technologies, Boulder, CO) operates at 632.8 nm and measures light scattering between 35° and 145° collecting light from the direct and the reflected light beam (angular range 35°–120° and 60°–145°, respectively), so that light scattered between 60° and 120° need to be counted twice. It derives the particle number size distribution over 31 channels between 0.1 and 3.0 μm in optical equivalent diameter (e.g., Liu et al., 1992; Reid and Hobbs, 1998; Rosenberg et al., 2012).
2. The Ultra High Sensitivity Aerosol Spectrometer (UHSAS, Droplet Measurement Technologies, Boulder, CO). This probe has a ground−based version but it is mostly used airborne (e.g., Cai et al., 2008; Petzold et al., 2013; Brock et al., 2016; Kupc et al., 2018). It operates at 1054 nm and provides the number size distribution of particles with D_{OE} ranging from 0.04 to 1 μm in 99 nominal size classes. The light−scattering sensing angle range (22°−158°) provided by Cai et al. (2008) has been subsequently corrected by Petzold et al. (2013) and Brock et al. (2016), who reported that the optically active range is from 33° to 148°, with a blind region between 75.2 and 104.8°.
3. The Forward Scattering Spectrometer Probe (FSSP, Model 300, Droplet Measurement Technologies, Boulder, CO). This widely used aircraft probe measures light−scattering at 632.8 nm in an optically−active volume extending from 3 to 15° to retrieve the number size distribution in a nominal size range from 0.28 to 20.5 μm over 30 size classes (Baumgardner et al., 1992; Petzold et al., 2013).
4. The Cloud Droplet Probe (CDP, Model 300, Droplet Measurement Technologies, Boulder, CO) measures light−scattering at 658 nm in an optically−active volume extending from 4° to 12° to retrieve the number size distribution in a nominal size range from 2 to 50 μm over 30 size classes (Baumgardner et al., 1992; Petzold et al., 2013).
5. The ground−based GRIMM and airborne Sky− GRIMM OPCs (Grimm Aerosol Technik, models 1.109 and 1.129, Ainring, Germany) retrieve the particle number distribution over 31 size classes distributed between 0.25 and 32 μm nominal diameter. These particle counters operate at 655 nm. These OPCs measure light scattered by the direct beam is 30°−150° and by the reflected beam between 81° and 98° thanks to two face−to face

https://doi.org/10.5194/ar-2026-20
Preprint. Discussion started: 11 June 2026

parabolic mirrors (opening angles of 120° and 18°, respectively) collecting light around a mean scattering angle of 90° (F. Schneider, personal communication). As for the PCASP, the light scattered between 81° and 98° has twice the weight relative to the intensity within 30°-81° and 98°-150°.

Table 1 summarizes the nominal technical specification of the different OPCs considered in this study.

Table 1. *Nominal technical specifications (nominal size bins corresponding to the optical diameters D_{EO} at reference refractive index, operating light−source spectral domain, and opening angles of the sensing volume, material used for reference calibration, and reference publication) for the OPCs considered in this paper. PSL stands for particle sphere latex.*

Instrument	Bin size D_{OE} (µm)	Wavelength (nm)	Range of scattered light	Calibration	Primary reference
PCASP−100X	0.1−3.0 (31 channels)	632.8 (unpolarised)	35°–120°(direct beam) + 60°–145° (reflected beam)	PSL (1.59−0*i*)	Liu et al. (1992)
UHSAS	0.06 – 1 (99 channels)	1054 (linearly polarised)	33° −75.2° + 104.8°−148°	PSL (1.572−0.001*i*)	Cai et al. (2008)
FSSP−300	0.275−20.5 (30 channels)	632.8 (unpolarised)	3°−15°	PSL (1.59−0*i*)	Baumgardner et al. (1992)
CDP-300	2−50 (30 channels)	658 (unpolarised)	4°−12°	Glass beads (1.59−0*i*)	Lance et al. (2010)
GRIMM model 1.109	0.25 – 32 (31 channels)	655[$] (unpolarised)	30°−150° (direct beam) + 81°−98° (reflected beam)	PSL (1.59−0*i*)	Heim et al. (2008)
Sky−GRIMM model 1.129[#]	0.25 – 32 (31 channels)	655[$] (unpolarised)	30°−150° (direct beam) + 81°−98° (reflected beam)	PSL (1.59−0*i*)	Grimm and Eatough (2009)

[$] Company specifications. Heim et al. (2008) reported that the working wavelength of the GRIMM 1.109 is 683 nm.
[#] The technical characteristics of the GRIMM and Sky−GRIMM OPCs relevant to this paper are identical and calculations performed once hold for both of them.

Table 1 also reports the reference material used for the calibration for each of the OPCs. National Institute of Standards and Technology (NIST)-certified polystyrene latex spheres (PSL) are used for the UHSAS, PCASP−100, FSSP−300, and GRIMM 1.109/Sky−GRIMM 1.129. The CDP is calibrated with glass beads. The refractive index of PSL, also reported in Table 1, has been measured by Velazco-Roa and Thennadil (2007) and Nikolov and Ivanov (2000).

For each size bin, the midpoint diameter D_{mid} is defined as

$$D_{mid} = \sqrt{D_{bin,lower} * D_{bin,upper}} \quad (1)$$

https://doi.org/10.5194/ar-2026-20
Preprint. Discussion started: 11 June 2026

where $D_{bin,lower}$ and $D_{bin,upper}$ are the lower and the upper limits of the bin diameter, respectively. The bin width dlog$D$ is defined as

$$dlogD = log\left(\frac{D_{bin,upper}}{D_{bin,lower}}\right) \quad (2)$$

where log indicates base 10.

2.2. Optical calculations

Following Rosenberg et al. (2012), the scattering cross−section C_{sca} for all instrument except the UHSAS can be calculated as

$$C_{sca}(\lambda) = \frac{\pi}{k^2}\int_0^{2\pi}\int_{\theta_{min}}^{\theta_{max}}\left(|\,S1(\theta,\lambda,D_p,m)\,|^2+|\,S2(\theta,\lambda,\,D_p,m)\,|^2\right)\sin(\theta)w_{optics}(\theta,\varphi)d\theta d\varphi \quad (3)$$

where

- λ is the operating wavelength of the OPC
- D_p is the particle diameter,
- m is the particle complex refractive index,
- $S1$ is the light−scattering intensity polarized in the parallel plane and $S2$ in the perpendicular plane. Their squared sum, integrated over the scattering angle range characteristic of the OPCs is the total light intensity seen by the instrument;
- θ is the angle between the incident laser beam and the scattering direction,
- φ is the direction of the scattered radiation around the incident beam,
- $w_{optics}(\theta,\varphi)$ is a weighting function defined by the optical geometry of the OPC. As defined by Rosenberg et al. (2012), $w_{optics}(\theta,\varphi)$ takes into account the fact that, at certain angles, the PCASP and GRIMM/Sky−GRIMM measure scattered light both directly and after reflection by a mirror. In the case of rotational symmetry around the laser beam, $w_{optics}(\theta,\varphi)$ is a function of the scattering angle θ only.

For the UHSAS, using polarized light, the scattering cross−section C_{sca} is

$$C_{sca}(\lambda) = \frac{\pi}{k^2}\int_0^{2\pi}\int_{\theta_{min}}^{\theta_{max}}\left(|\,S1(\theta,\lambda,D_p,m)\sin^2\varphi\,|^2+|\,S2(\theta,\lambda,\,D_p,m)\cos^2\varphi\,|^2\right)\sin(\theta)w_{optics}(\theta,\varphi)d\theta d\varphi \quad (4)$$

https://doi.org/10.5194/ar-2026-20
Preprint. Discussion started: 11 June 2026

All calculations use Mie theory for homogeneous spherical particles, calculated according to Bohren and Huffman (2007). The particle diameter D_p in Equations 3 and 4 is varied between 0.02 and 200 µm in logarithmically−equal steps of 0.004 (1001 values). The real part n of the complex refractive index is varied between 1.33 and 1.75 (in steps of Δn = 0.01) and the imaginary part k from 0.0 to 0.4 (steps of Δk = 0.001) encompassing the range of values expected for atmospheric aerosols (e.g., Shettle and Fenn, 1992) at the working wavelengths of the OPCs. Individual aerosol species such as black carbon might have higher imaginary part k (~0.96) in the near infrared (Moteki et al., 2023), but in ambient conditions they are generally found in less absorbing mixtures.

2.3. Determination of the D_{OE} to D_{geom} correction

The procedure to determine the geometric diameter (D_{geom}) for the ambient refractive index is illustrated in Fig. 1, using the PCASP as an example.

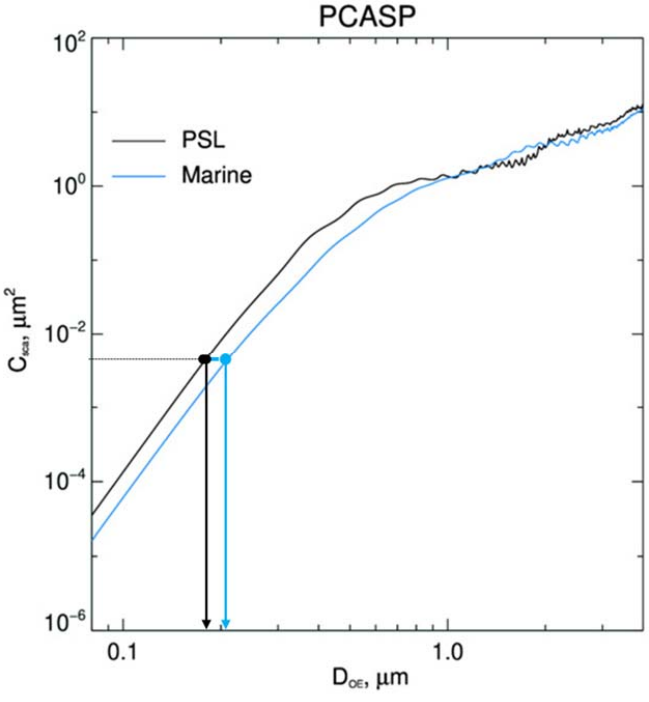

Figure 1. Scattering cross section C_{sca} as a function of particle diameter calculated using Mie theory for the PCASP. The black line represents the C_{sca} for the calibration particles (PSL). The light blue line represents the C_{sca} for marine aerosols (m = 1.38 – 0.001i). The small vertical grey lines represent the bin edges for the nominal calibration particles.

The initial step consists in identifying the C_{sca} values corresponding to each nominal D_{OE} bin size ($D_{bin,lower}$ and $D_{bin,upper}$) for the calibration m value, geometry and operating wavelength of

https://doi.org/10.5194/ar-2026-20
Preprint. Discussion started: 11 June 2026

the OPC, calculated as explained in Sect. 2.2. As an example, one specific pair of C_{sca}-D_{OE} value is indicated by the black arrows in Fig. 1. The equivalent of those C_{sca} values are then searched on the curves corresponding to the ambient complex refractive index *m*, in our example that corresponding to marine aerosols, so to determine the new diameter value. Numerically, this is achieved by minimizing the difference between the nominal $C_{sca,bin,lower}$ and $C_{sca,bin,\ upper}$ with respect to the C_{sca} values corresponding to the atmospheric *m* value. These will represent the new limits of the bin diameter for the D_{geom} bin. The procedure is repeated for each bin of the OPC and the upper and lower bin limits are used to calculate the mid-point diameter and bin width by applying Eq. (1)-(2).

3. Results and discussion

While we refer the reader to the extensive discussions in Petzold et al. (2013), Moore et al. (2021), and Lewis et al. (2026), amongst others, this section describes some elements of analysis to understand the size correction factors presented in the datasets. To do so, we use four examples: non−absorbing material used for calibration (polystyrene latex spheres or equivalent light−scattering material; OPC-dependent), mineral dust (m = 1.53 – 0.003i; e.g., Fig. 8 in Di Biagio et al., 2019), urban aerosols (m = 1.56 – 0.087i; e.g., Radney and Zangmeister, 2018), and marine aerosols (m = 1.38 – 0.001i; e.g., Zieger et al., 2017).

3.1. Dependence of scattering cross section to size and complex refractive index

Figure 2 shows the behavior of the C_{sca} functions with particle diameter for the example *m* values.

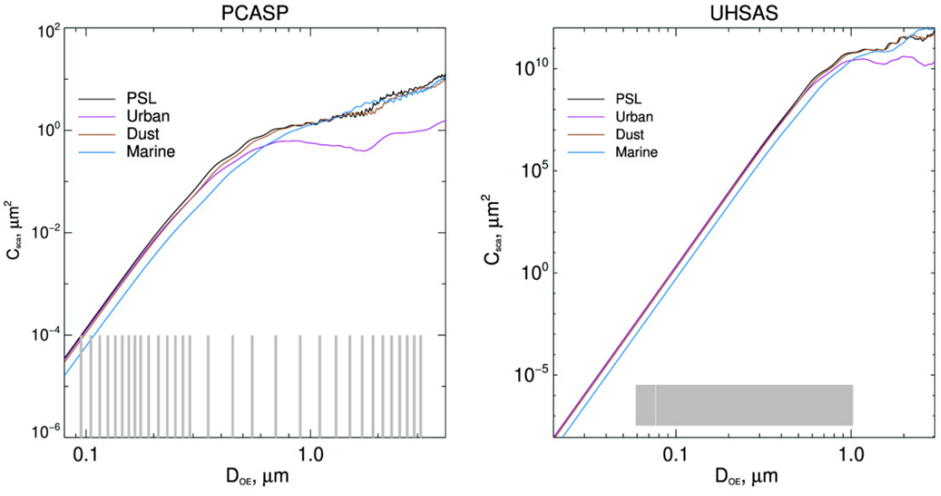

https://doi.org/10.5194/ar-2026-20
Preprint. Discussion started: 11 June 2026

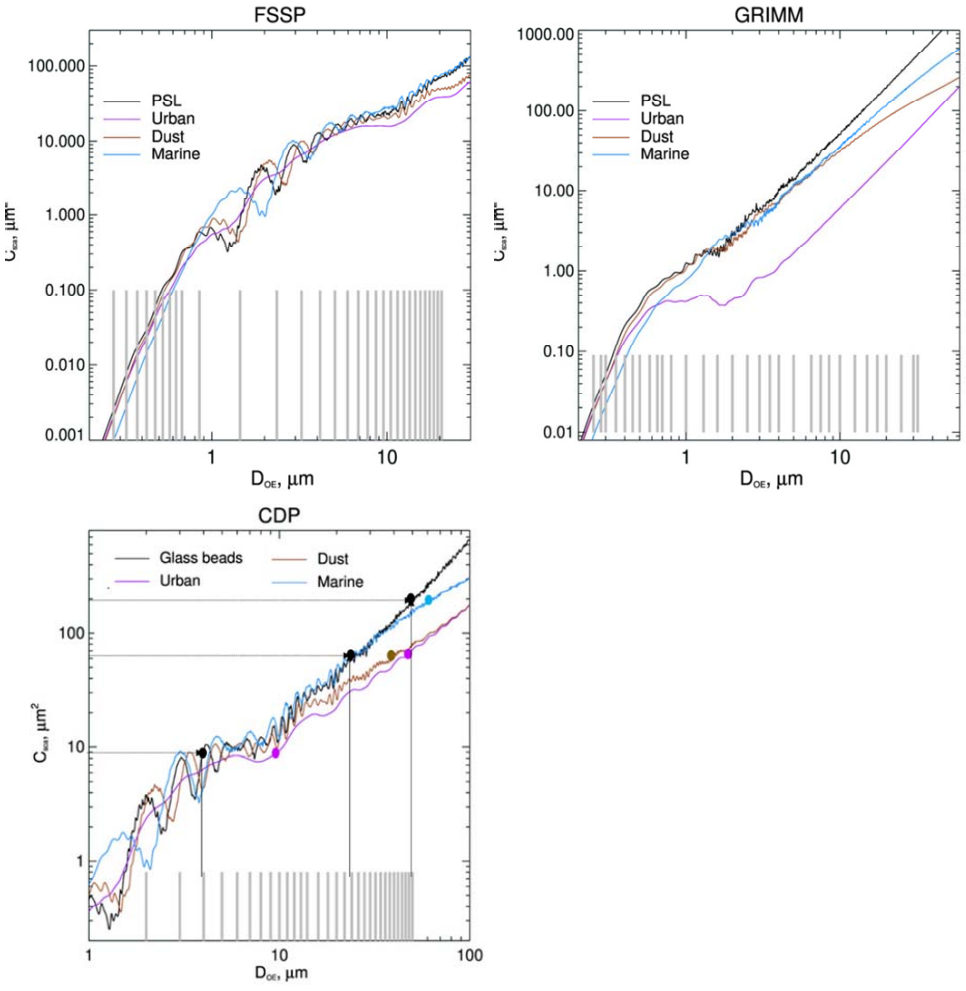

269 ***Figure 2.*** *Scattering cross section C_{sca} as a function of particle diameter calculated using Mie theory for the OPCs*
270 *considered in this paper. The black lines represent C_{sca} for the calibration particles (PSL or glass beads). The purple*
271 *lines represent the C_{sca} function for absorbing urban aerosols (m = 1.56 – 0.087i), while the brown lines represent*
272 *C_{sca} for moderately−absorbing mineral dust (m = 1.53 – 0.003i), and the light blue lines represent C_{sca} for marine*
273 *aerosols (m = 1.38 – 0.001i).. The small vertical grey lines represent the bin edges for each OPC.*

274

275 Figure 2 well illustrates the general problematic associated to D_{OE} to D_{geom} correction: due to
276 non-monotonic behavior and Mie oscillations, the C_{sca} calculated from the nominal bin value
277 can correspond to several particle diameters. As a consequence, for a given value of *m*, there
278 is an ambiguity in sizing particles in certain diameter ranges, so that it is not always possible
279 to infer the particle size on the entire nominal size range of each OPC. The oscillations tend to
280 smooth for absorbing aerosols, as shown for the urban aerosol type. The C_{sca} functions of

https://doi.org/10.5194/ar-2026-20
Preprint. Discussion started: 11 June 2026

wide−angle probes (PCASP, UHSAS, and GRIMM/Sky−GRIMM) are less affected by Mie oscillations than forward−scattering probes (FSSP−300 and CDP), and their behavior tends to be monotonic with size. However, the PCASP and the GRIMM/Sky−GRIMM curves become flatter around 1 µm as the imaginary part of the *m* increases. In practical terms, this precludes their possibility of sizing absorbing particles in the range between 0.6 and 2 µm. For FSSP−300 and CDP, the determination of particle size is problematic in the range between 1 and 5 µm. On the contrary, the C_{sca} of UHSAS is monotonic with particle size on almost the entire size range and that regardless of particle *m*, as discussed in Moore et al. (2021). These considerations are generalized in Fig. S1 in the supplementary material showing the size-dependent scattering cross sections for the whole range of complex refractive index investigated in the database.

3.2. Equivalence in particle size

Figure 2 henceforth helps understanding the difficulties in finding an equivalence between D_{OE} at the reference *m* and D_{geo} at the aerosol *m.* As described in Sect. 2.3, the first step of the procedure consists in calculating, for each value of D_{OE} and for each value of refractive index, the C_{sca} corresponding to the geometry and the operating wavelength of the OPC. The second step consists in finding at which value of diameter corresponds each calculated value of C_{sca}, depending on the refractive index. The curve for the CDP can be analyzed to do so. A dotted horizontal line in Figure 2 takes the example of three given values of C_{sca} corresponding to three bin boundaries (4, 24 and 50 µm) in the calibration curve. Due to non-monotonic behavior and Mie oscillations, for the glass beads, marine and dust aerosols the C_{sca} values may correspond to several particle diameters. For the urban aerosols, oscillations are smoothed out because the imaginary part of the refractive index. However, sizing the bins results in a much larger D_{geo}, due to the lower C_{sca} (this is the case for dust too). The third step consists henceforth in selecting, for each refractive index, the best guess of corrected particle diameter (D_{geo}). Our choice is to select the minimum value of calculated diameter, that is, the value of D_{geo} closest to the initial D_{OE} value. In the current example, the calculated D_{geo} would be 11 µm for urban aerosols, 4.8 µm for mineral dust and 4.2 µm for marine aerosols.

The result of the procedure, that is, the scatterplot of the geometric bin size boundary corresponding to the atmospheric *m* of mineral dust, urban and marine aerosols, with respect to the optical-equivalent bin size boundary obtained for the calibration *m* is illustrated in Fig. 3.

https://doi.org/10.5194/ar-2026-20
Preprint. Discussion started: 11 June 2026

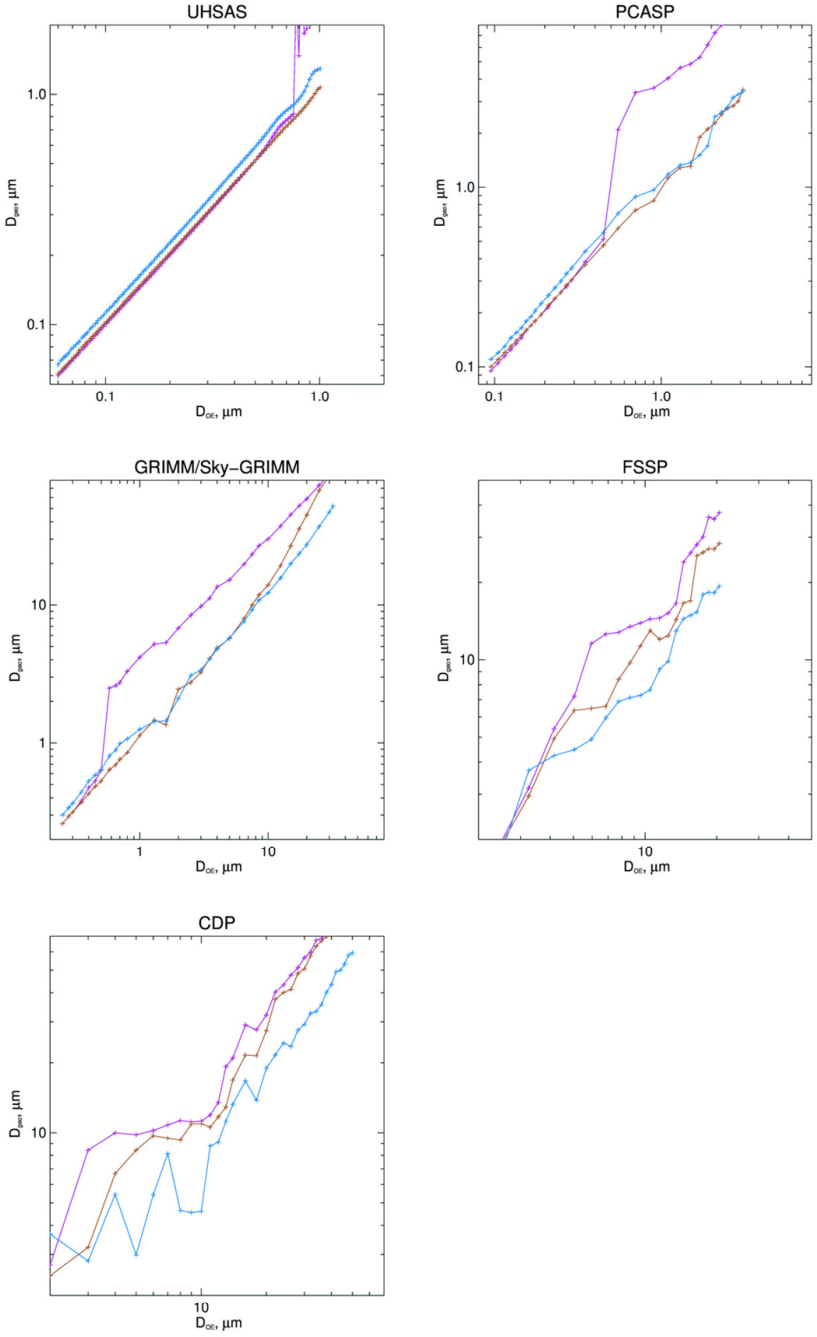

312 ***Figure 3.*** *For each OPC: Scatterplot of geometric−equivalent bin size boundary (D_{geo}) corresponding to the complex*
313 *refractive index of the example aerosol types (mineral dust, urban and marine) with respect to the optical−equivalent*
314 *bin size boundary (D_{OE}) obtained if the calibration m is used. The colour code is: black line for calibration, light blue*
315 *line for marine aerosol, purple line for urban aerosol and brown line for mineral dust aerosol.*
316

https://doi.org/10.5194/ar-2026-20
Preprint. Discussion started: 11 June 2026

Figure 3 illustrates to which extent, as a result of differences in the scattering cross-sections, the corrected diameter may differ from the calibration one, in particular for light-absorbing particles. For UHSAS, differences are mostly evident in the upper part of the sizing range. The changes of the corrected diameter with size are not linear but depend on the size range. In general terms, the largest differences between the uncorrected and the corrected diameter occur for particles larger than 1 micron. A zone of non-linearity appears around 1 μm for OPCs measuring side scattering (i.e. PCASP and GRIMM/Sky-GRIMM), and between 5 and 10 μm for forward-scattering probes such as the FSSP and the CDP. Instances when the corrected size oscillate are also observed (for example, CDP for marine aerosols). There are size ranges at which the OPC cannot properly size particles, as result of the independence of C_{sca} on size shown in Figure 2. The blind region depends on the OPC. For the CDP, it is comprised between 4 and 10 μm, for the FSSP it is around 6 and 10 μm, for the GRIMM and the PCASP is between 1 and 2 μm. Evidently, these ranges of values change with the complex refractive index, that on its turn, depends on aerosol type. As already discussed by Lewis et al. (2026), the width of the size classes (dlog$D$) becomes irregular, and even result in negative values for those classes when the corrected size of the upper bin (at atmospheric m) is smaller than the corrected size of the lower bin (not shown). These instances can easily be identified by the values of dlog$D$ that are negative, corresponding to the corrected size of the upper bin (at atmospheric CRI) being smaller than the corrected size of the lower bin (Eq. 3).

3.3. Representation of the size distribution

Figure 4 provides illustration of the possible consequences in the representation of the particle number size distribution considering or not the composition-dependent size correction factors. To do so, a synthetic number size distribution consisting in a two-mode lognormal centered at 150 nm (sigma = 1.6) and 1 μm (sigma = 1.8) is considered.

https://doi.org/10.5194/ar-2026-20
Preprint. Discussion started: 11 June 2026

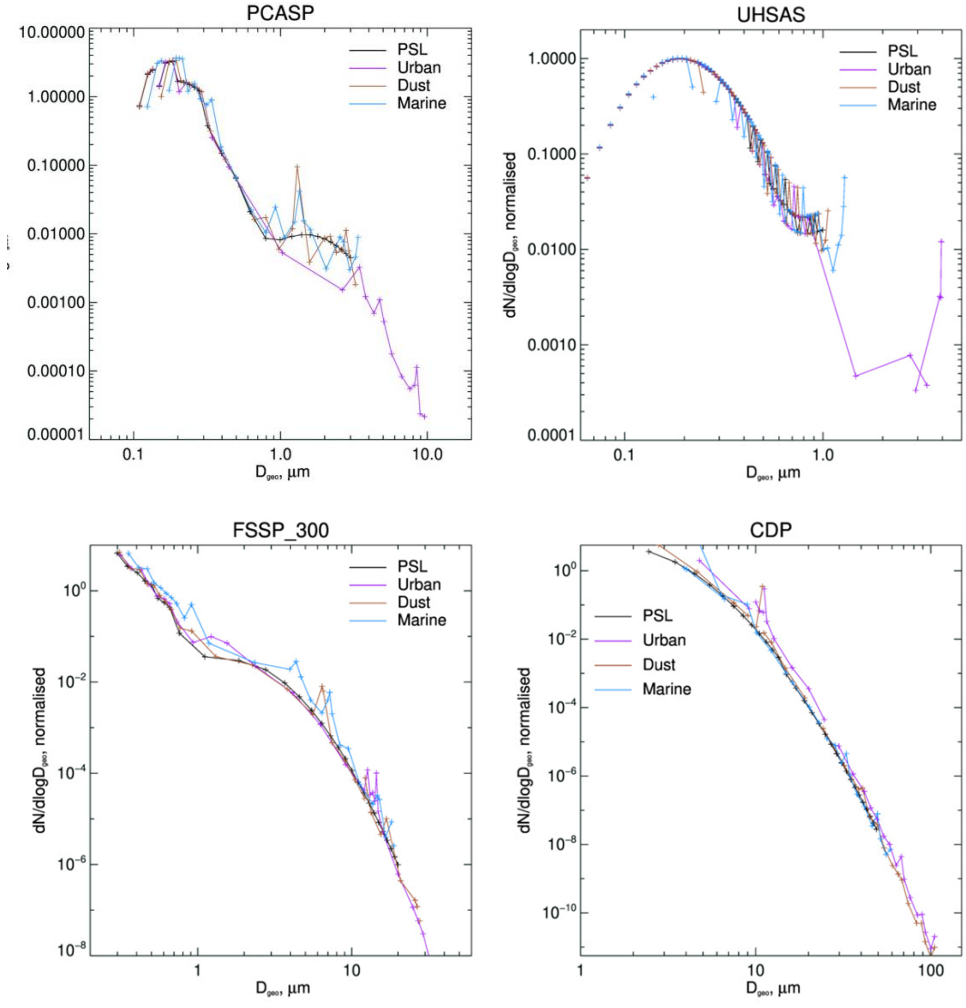

https://doi.org/10.5194/ar-2026-20
Preprint. Discussion started: 11 June 2026

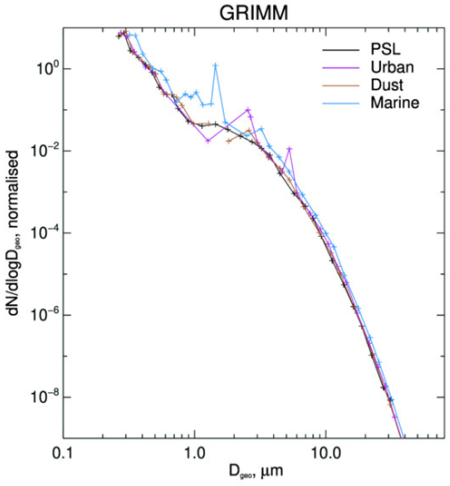

Figure 4. *Representation of a bi-modal log−normal size distribution by the OPCs considered in this paper, taking into account the corrected bin diameter for the example aerosol types (mineral dust, urban and marine).*

First of all, considering a composition-dependent correction factor redistributes particles in different classes and may result in artificially enlarged range of the measured size distribution, notably for absorbing particles. Care should be taken in normalizing the corrected particle size distribution to make sure that the total particle number is conserved. Secondly, as discussed in detail by Lewis et al. (2026) for the GRIMM and the UHSAS, correcting for the refractive index may induce spikes and discontinuities in correspondence to irregularities in the width of the bin sizes. These discontinuities appear as spurious narrow modes, which depending on their position in size, might have a large impact in the calculation of the total mass, or optical properties. While they most likely and severe for OPCs with high size resolution, it is worth noticing that, for these reasons, almost all OPCs have larger size bins at sizes where the C_{sca} curves flatten or are most affected by oscillations.

5. Summary and recommendations

By this paper, we describe a set of standardized corrections of particle sizing by OPC instruments in order to account for the dependence of angular scattering on particle composition, as represented by the particle complex refractive index *m*. This dataset of corrections is based on the simple assumption of homogeneous spherical particles and the use of Mie theory, and considers nominal OPC characteristics in terms of scattering angles of the sensing volume and wavelengths of the light sources. The approach covers the range of refractive indices expected for atmospheric aerosols.

In general terms, the analyses described confirm that research−grade OPC probes perform very well for the size ranges and for the particle types for which they were designed, as a result

https://doi.org/10.5194/ar-2026-20
Preprint. Discussion started: 11 June 2026

of careful design by experts in the field (see references in Table 1, and the overview of Wendisch and Brenguier (2003)). The behavior of light scattering intensity with size indicates that the UHSAS performs very well for submicron particles with diameters less than 800 nm, regardless of their refractive index, and represents a very significant improvement compared to the PCASP instrument that operates on a similar, albeit more reduced size range. The FSSP, CDP, and GRIMM/Sky−OPC should be used to size particles larger than approximately 1 µm. The GRIMM/Sky−GRIMM can be problematic in the range 1-2 µm. The FSSP and CDP can be problematic below 10 µm.

We recommend the users consider very carefully instances when light scattering is not monotonic with size, and use care when selecting the method for eliminating them. Discontinuities and artefact may be corrected by eliminating or reducing the amplitude of ripples and oscillations by smoothing or fitting the theoretical C_{sca} curves provided in the OPC_intensity_real_imag.txt files, prior resampling them at the desired size bins (e.g., Liu et al., 1974; Hand and Kreidenweis, 2002; Covert et al., 1990; Johnson et al., 2008; Lance et al., 2010). Other approaches consist in grouping or widening the bins of the OPCs (e.g., Johnson and Osborne, 2011), or exclude specific size ranges (e.g., Denjean et al., 2016), notably when the recalculated values of dlog$D$ are negative.

We recommend users to combine as much as possible the retrieval of the particle size distribution from OPCs with concurrent, complementary measurements (e.g. particles sizers based on electrical mobility or aerodynamics, lidar measures of the backscattering vertical profile, gravimetric or composition measurements providing the mass concentration and composition) for optical and/or mass closure in order to ensure the robustness and consistency of the dataset, and improved knowledge of the complex refractive index. Finally, and in order to make the best use of the possibilities offered by open data policies, we also recommend that users, whenever possible, to make contact with instrument operators to verify the specifics of the OPCs, their calibration, and their performance during field operations.

Finally, the significant sensitivity of the light scattering intensity C_{sca} to the particle complex refractive index drives the recommendation that diameters corrected for the m should be used rather than the calibration diameters even if particle m is not precisely known. Even with an approximate assumption of the particle origin (i.e. wind direction, time of day, season of year, air mass trajectory), assuming an aerosol type and/or m based on these other environmental conditions and using the corresponding m-corrected diameter is likely to be more accurate than using the calibration diameters. The dataset presented in this paper can also be used without any knowledge of the particle refractive index, or to deduce the refractive index of the aerosol if other instruments are available for closure or if more than one OPC are used. This approach can also provide uncertainty or sensitivity of size distribution estimates.

https://doi.org/10.5194/ar-2026-20
Preprint. Discussion started: 11 June 2026

The approach presented in this work could be extended to other research-grade OPC, such as the Palas® WELAS operating with white light (Heim et al., 2008), as well as to low-cost sensors, provided that their geometrical characteristics are known with sufficient precision (Hagan and Kroll, 2020). Further work should also address the impact of morphology and provide a shape−dependent formulation to optimize the correction to non-spherical particles such as mineral dust, soot, salts and crystals.

Data availability

Optical calculations with Mie theory for homogeneous spherical particles have been performed with the IDL mie_single.pro routine available at http://www.eodg.atm.ox.ac.uk/MIE/mie_single.html).

The datasets described in this paper are accessible via the EasyData portal maintained by the French national data center DATA TERRA at https://doi.org/10.57932/36ba1ebc-604c-4d6c-a3a8-7dc2de952241 (last accessed: 21/05/2026). The dataset consists in ten files in zip format, corresponding to the five OPCs considered in this study and to two types of ASCII files:

1/ For each OPC, the values of scattering cross section C_{sca} for particle diameters comprised between 0.02 and 200 µm in logarithmically−equal steps of 0.004 and as a function of m (n=1.33−1.75; Δn=0.01, k=0.0-0.4; Δk=0.001) are provided in ascii files whose generic name is OPC_intensity_real_imag.txt, where *OPC* is the acronym of the particle counter, *real* is the value of the real part and *imag* is the imaginary part of the complex refractive index. Each file contains four columns, namely

- the real part of m
- the imaginary part of m
- the particle diameter used in Equations 1 and 2 (in µm)
- the corresponding value of C_{sca} (in µm^2)

2/ The values of the corrected bin diameter as a function of m (n=1.33−1.75; Δn=0.01, k=0.0-0.4; Δk=0.001) are provided in text files whose generic name is OPC_Diameter_real_imag.out, where *OPC* is the acronym of the particle counter, *real* is the value of the real part of the *CRI*, and *imag* is the imaginary part of the m. Each file contains four columns, namely

- the nominal bin diameter (in µm) of the calibration m
- the bin diameter (in µm) calculated for the atmospheric m
- the bin midpoint diameter (D_{mid}, in µm) calculated for the atmospheric m

the bin width (dlog$D$) calculated for the atmospheric m.

Competing interests. The authors declare no conflict of interest.

https://doi.org/10.5194/ar-2026-20
Preprint. Discussion started: 11 June 2026

Special issue statement. This article is not part of a special issue. It is not associated with a conference.

Author contribution. PF and CDB designed the research, performed the optical calculations, and wrote the manuscript.

Acknowledgments.

The help of Guillaume Brissebrat (CNRS/DATA TERRA/Aeris), and Hélène Bressan (GaiaData BRGM) in creating the DOIs for the different datasets is gratefully acknowledged. Thanks are due to Marc Daniel Mallet (University of Tasmania), Jasper F. Kok and and Yue Huang (ULCA) for useful discussions on an earlier version of the manuscript.

Financial support

This work was conducted within the DustClim project, part of ERA4CS, an ERA−NET initiated by JPI Climate, and funded by FORMAS (SE), DLR (DE), BMWFW (AT), IFD (DK), MINECO (ES), ANR (FR) with co−funding by the European Union (Grant 690462).

https://doi.org/10.5194/ar-2026-20
Preprint. Discussion started: 11 June 2026

References

Baron, P. A., and Willeke, K.: Aerosol measurement: Principles, techniques and applications, 2nd ed., John Wiley and Sons, New York, 2001.

Baumgardner, D., Dye, J. E., Gandrud, B. W., and Knollenberg, R. G.: Interpretation of measurements made by the forward scattering spectrometer probe (FSSP−300) during the Airborne Arctic Stratospheric Expedition, Journal of Geophysical Research: Atmospheres, 97, 8035−8046, https://doi.org/10.1029/91JD02728, 1992.

Baumgardner, D., Jonsson, H., Dawson, W., O'Connor, D., and Newton, R.: The cloud, aerosol and precipitation spectrometer: a new instrument for cloud investigations, Atmospheric Research, 59−60, 251−264, https://doi.org/10.1016/S0169−8095(01)00119−3, 2001.

Bohren, C. F., and Huffman, D. R.: Absorption and Scattering of Light by Small Particles, Wiley−VCH Verlag GmbH, 1983.

Bonazza, A., De Nuntiis, P., Mandrioli, P. and Sabbioni, C. (2017). Aerosol Impact on Cultural Heritage: Deterioration Processes and Strategies for Preventive Conservation. In Atmospheric Aerosols (eds C. Tomasi, S. Fuzzi and A. Kokhanovsky). https://doi.org/10.1002/9783527336449.ch11

Boucher, O., Randall, D., Artaxo, P., Bretherton, C., Feingold, G., Forster, P., Kerminen, V.−M., Kon−do, Y., Liao, H., Lohmann, U., Rasch, P., Satheesh, S.K., Sherwood, S., Stevens B., and Zhang X. Y., Clouds and Aerosols. In: Climate Change 2013: The Physical Science Basis. Contribu−tion of Working Group I to the Fifth Assessment Report of the Intergovernmental Panel on Climate Change [Stocker, T.F., D. Qin, G.−K. Plattner, M. Tignor, S.K. Allen, J. Boschung, A. Nauels, Y. Xia, V. Bex and P.M. Midgley (eds.)]. Cambridge University Press, Cambridge, United Kingdom and New York, NY, USA, 2013.

Brock, C. A., Wagner, N. L., Anderson, B. E., Attwood, A. R., Beyersdorf, A., Campuzano−Jost, P., Carlton, A. G., Day, D. A., Diskin, G. S., Gordon, T. D., Jimenez, J. L., Lack, D. A., Liao, J., Markovic, M. Z., Middlebrook, A. M., Ng, N. L., Perring, A. E., Richardson, M. S., Schwarz, J. P., Washenfelder, R. A., Welti, A., Xu, L., Ziemba, L. D., and Murphy, D. M.: Aerosol optical properties in the southeastern United States in summer – Part 1: Hygroscopic growth, Atmos. Chem. Phys., 16, 4987–5007, https://doi.org/10.5194/acp−16−4987−2016, 2016.

Brock, C. A., Williamson, C., Kupc, A., Froyd, K. D., Erdesz, F., Wagner, N., Richardson, M., Schwarz, J. P., Gao, R.−S., Katich, J. M., Campuzano−Jost, P., Nault, B. A., Schroder, J. C., Jimenez, J. L., Weinzierl, B., Dollner, M., Bui, T., and Murphy, D. M.: Aerosol size distributions during the Atmospheric Tomography Mission (ATom): methods, uncertainties, and data products, Atmos. Meas. Tech., 12, 3081–3099, https://doi.org/10.5194/amt−12−3081−2019, 2019.

Cai, Y., Montague, D. C., Mooiweer−Bryan, W., and Deshler, T.: Performance characteristics of the ultra high sensitivity aerosol spectrometer for particles between 55 and 800 nm: Laboratory and field studies, J. Aerosol Sci., 39, 759–769, doi:10.1016/j.jaerosci.2008.04.007, 2008.

Collins, D. R., Johnsson, H. H., Seinfeld, J. H., Flagan, R. C., Gassó, S., Hegg, D. A., Russell, P. B., Schmid, B., Livingston, J. M., Öström, E., Noone, K. J., Russell, L. M., and Putaud, J. P.: In situ aerosol size distributions and clear column radiative closure during ACE−2, Tellus, 52B, 498 − 525, 2000.

Covert, D. S., Heintzenberg, J., and Hansson, H. C.: Electrooptical detection of external mixtures in aerosols, Aerosol Sci. Tech., 12, 446–456, 1990.

Crilley, L. R., Shaw, M., Pound, R., Kramer, L. J., Price, R., Young, S., Lewis, A. C. and Pope, F. D.: Evaluation of a low−cost optical particle counter (Alphasense OPC−N2) for 28ambient air monitoring, Atmospheric Measurement Techniques, 11(2), 709–720, 29doi:https://doi.org/10.5194/amt−11−709−2018, 2018.

Denjean, C., Cassola, F., Mazzino, A., Triquet, S., Chevaillier, S., Grand, N., Bourrianne, T., Momboisse, G., Sellegri, K., Schwarzenbock, A., Freney, E., Mallet, M., and Formenti, P.: Size distribution and optical properties of mineral dust aerosols transported in the western Mediterranean, Atmos. Chem. Phys., 16, 1081−1104, doi:10.5194/acp−16−1081−2016, 2016.

Di Biagio, C., L. Doppler, C. Gaimoz, N. Grand, G. Ancellet, J.−C. Raut, M. Beekmann, A. Borbon, K. Sartelet, J.−L. Attié, F. Ravetta, P. Formenti, Continental pollution in the Western Mediterranean

https://doi.org/10.5194/ar-2026-20
Preprint. Discussion started: 11 June 2026

basin: vertical profiles of aerosol and trace gases measured over the sea during TRAQA 2012 and SAFMED 2013, Atmos. Chem. Phys., 15, 9611–9630, doi:10.5194/acp−15−9611−2015, 2015

Di Biagio, C., Formenti, P., Balkanski, Y., Caponi, L., Cazaunau, M., Pangui, E., Journet, E., Nowak, S., Caquineau, S., Andreae, M. O., Kandler, K., Saeed, T., Piketh, S., Seibert, D., Williams, E., and Doussin, J.−F.: Global scale variability of the mineral dust long−wave refractive index: a new dataset of in situ measurements for climate modeling and remote sensing, Atmos. Chem. Phys., 17, 1901−1929, doi:10.5194/acp−17−1901−2017, 2017.

Dubovik, O., A. Sinyuk, T. Lapyonok, B. N. Holben, M. Mishchenko, P. Yang, T. F. Eck, Volten, H., Muñoz, O., Veihelmann, B., W. J. van der Zande, Leon, J.−F., Sorokin, M., and Slutsker, I.: Application of spheroid models to account for aerosol particle nonsphericity in remote sensing of desert dust, J. Geophys. Res., 111, doi:10.1029/2005JD006619, 2006.

Flores, J. M., Trainic, M., Borrmann, S., and Rudich, Y.: Effective broadband refractive index retrieval by a white light optical particle counter, Physical Chemistry Chemical Physics, 11, 7943−7950, 2009.

Garvey, D. M., and R. G. Pinnick, Response Characteristics of the Particle Measuring Systems Active Scattering Aerosol Spectrometer Probe (ASASP–X), Aerosol Science and Technology, 2:4, 477−488, DOI: 10.1080/02786828308958651(1983).

Grimm, H., and Eatough, D. J.: Aerosol measurement: the use of optical light scattering for the determination of particulate size distribution, and particulate mass, including the semi−volatile fraction, J. Air Waste Manag. Assoc., 59, 101–107, doi:10.3155/1047−3289.59.1.101, 2009.

Formenti, P., and Di Biagio, C., Look−up tables resolved by complex refractive index to correct particle sizes measured by common research−grade optical particle counters.https://doi.org/10.57932/36ba1ebc-604c-4d6c-a3a8-7dc2de952241, 2026.

Hagan, D. H. and Kroll, J. H.: Assessing the accuracy of low-cost optical particle sensors using a physics-based approach, Atmos. Meas. Tech., 13, 6343–6355, https://doi.org/10.5194/amt-13-6343-2020, 2020.

Hand, J. L. and Kreidenweis, S. M.: A New Method for Retrieving Particle Refractive Index and Effective Density from Aerosol Size Distribution Data, Aerosol Sci. Tech., 36, 1012–1026, 2002.

Haywood, J. M., Osborne, S. R., Francis, P. N., Keil, A., Formenti, P., Andreae, M. O., and Kaye, P. H.: The mean physical and optical properties of regional haze dominated by biomass burning aerosol measured from the C−130 aircraft during SAFARI 2000, J. Geophys. Res., 108, 8473, 10.1029/2002jd002226, 2003a.

Haywood, J. M., Francis, P., Osborne, S., Glew, M., Loeb, N., Highwood, E., Tanré, D., Myhre, G., Formenti, P., and Hirst, E.: Radiative properties and direct radiative effect of Saharan dust measured by the C−130 aircraft during SHADE: 1. Solar spectrum, J. Geophys. Res., 108, doi:10.1029/2002JD002687, doi:10.1029/2002JD002687, 2003b.

Heim, M., Mullins, B. J., Umhauer, H., and Kasper, G.: Performance evaluation of three optical particle counters with an efficient "multimodal" calibration method, Journal of Aerosol Science, 39, 1019−1031, 2008.

Hinds, W. C.: Aerosol technology: properties, behavior, and measurement of airborne particles, John Wiley & Sons, Chichester, 504 pp., 1999.

Howell, S. G., Freitag, S., Dobracki, A., Smirnow, N., and Sedlacek III, A. J.: Undersizing of aged African biomass burning aerosol by an ultra-high-sensitivity aerosol spectrometer, Atmos. Meas. Tech., 14, 7381–7404, https://doi.org/10.5194/amt-14-7381-2021, 2021.

Huang, Y., Kok, J. F., Kandler, K., Lindqvist, H., Nousiainen, T., Sakai, T., Adebiyi, A., and Jokinen, O.: Climate Models and Remote Sensing Retrievals Neglect Substantial Desert Dust Asphericity, Geophys. Res. Lett., 47, 475, e2019GL086592, 2020a, https://doi.org/10.1029/2019GL086592.

Huang, Y., Adebiyi, A. A., Formenti, P., & Kok, J. F. (2021). Linking the different diameter types of aspherical desert dust indicates that models underestimate coarse dust emission. Geophysical Research Letters, 48, e2020GL092054. https://doi.org/10.1029/2020GL092054

Kanakidou, M., Stelios Myriokefalitakis and Kostas Tsigaridis, Aerosols in atmospheric chemistry and biogeochemical cycles of nutrients, Environmental Research Letters, 13, 2018

https://doi.org/10.5194/ar-2026-20
Preprint. Discussion started: 11 June 2026

Kandler, K. et al. (2009), Size distribution, mass concentration, chemical and mineralogical composition and derived optical parameters of the boundary layer aerosol at Tinfou, Morocco, during SAMUM 2006, Tellus, Ser. B Chem. Phys. Meteorol., 61(1), 32–50, doi:10.1111/j.1600-0889.2008.00385.x.

Kok, J. F., A. A. Adebiyi, S. Albani, Y. Balkanski, R. Checa-Garcia, M. Chin, P. R. Colarco, D. S. Hamilton, Y. Huang, A. Ito, M. Klose, D. M. Leung, L. Li, N. M. Mahowald, R. L. Miller, V. Obiso, C. Pérez García-Pando, A. Rocha-Lima, J. S. Wan, and C. A. Whicker (2021), Improved representation of the global dust cycle using observational constraints on dust properties and abundance, Atmospheric Chemistry and Physics, 21, 8127-67.

Kupc, A., Williamson, C., Wagner, N. L., Richardson, M., and Brock, C. A.: Modification, calibration, and performance of the Ultra-High Sensitivity Aerosol Spectrometer for particle size distribution and volatility measurements during the Atmospheric Tomography Mission (ATom) airborne campaign, Atmos. Meas. Tech., 11, 369–383, https://doi.org/10.5194/amt-11-369-2018, 2018.

Jaenicke, R. and Hanusch, T.: Simulation of the Optical Particle Counter Forward Scattering Spectrometer Probe 100 (FSSP−100), Aerosol Science and Technology, 18(4), 8309–322, doi:10.1080/02786829308959607, 1993

Johnson, B. T., S. R. Osborne, J. M. Haywood, and M. A. J. Harrison (2008), Aircraft measurements of biomass burning aerosol over West Africa during DABEX, J. Geophys. Res., 113, D00C06, doi:10.1029/2007JD009451

Johnson, B. T. and Osborne, S. R.: Physical and optical properties of mineral dust aerosol measured by aircraft during the GERBILS campaign, Q. J. Roy. Meteor. Soc., 137, 1117–1130, 2011.

Lance, S., Brock, C. A., Rogers, D., and Gordon, J. A.: Water droplet calibration of the Cloud Droplet Probe (CDP) and inflight performance in liquid, ice and mixed−phase clouds during ARCPAC, Atmos. Meas. Tech., 3, 1683–1706, doi:10.5194/amt−3−1683−2010, 2010.

Lewis, E. R., Gasparik, J. T., and Uin, J.: The impact of optical measurement techniques on measured aerosol particle size distributions, Aerosol Science and Technology, 1-13, 10.1080/02786826.2025.2609928, 2026.

Liu, B. Y. H., Berglund, R. N., and Agarwal, H. K.: Experimental studies of Optical Particle Counters, Atmos. Environ., 8, 717–732, 1974.

Liu, P. S. K., W. R. Leaitch, J. W. Strapp, and M. A. Wasey, Response of Particle Measuring Systems Airborne ASASP and PCASP to NaCl and Latex Particles, Aerosol Science and Technology, 16:2, 83−95, DOI: 10.1080/02786829208959539, 1992.

Moteki, N., Ohata, S., Yoshida, A., and Adachi, K.: Constraining the complex refractive index of black carbon particles using the complex forward-scattering amplitude, Aerosol Science and Technology, 57, 678-699, 10.1080/02786826.2023.2202243, 2023.

Meng, Z., P. Yang, G. W. Kattawar, L. Bi, K. N. Liou, and I. Laszlo (2010), Single−scattering properties of tri−axial ellipsoidal mineral dust aerosols: A database for application to radiative transfer calculations, J. Aerosol Sci., 41(5), 501–512, doi:10.1016/j.jaerosci.2010.02.008.10.1080/02786826.2019.1623863, 2020.

Mikuška, P., Večeřa, Z., Bartošíková, A., and Maenhaut, W.: Annular diffusion denuder for simultaneous removal of gaseous organic compounds and air oxidants during sampling of carbonaceous aerosols, Analytica Chimica Acta, 714, 68−75, https://doi.org/10.1016/j.aca.2011.11.054, 2012.

Moore, R. H., Wiggins, E. B., Ahern, A. T., Zimmerman, S., Montgomery, L., Campuzano Jost, P., Robinson, C. E., Ziemba, L. D., Winstead, E. L., Anderson, B. E., Brock, C. A., Brown, M. D., Chen, G., Crosbie, E. C., Guo, H., Jimenez, J. L., Jordan, C. E., Lyu, M., Nault, B. A., Rothfuss, N. E., Sanchez, K. J., Schueneman, M., Shingler, T. J., Shook, M. A., Thornhill, K. L., Wagner, N. L., and Wang, J.: Sizing response of the Ultra−High Sensitivity Aerosol Spectrometer (UHSAS) and Laser Aerosol Spectrometer (LAS) to changes in submicron aerosol composition and refractive index, Atmos. Meas. Tech., 14, 4517–4542, https://doi.org/10.5194/amt−14−4517−2021, 2021.

Nikolov, I. D., and Ivanov, C. D.: Optical plastic refractive measurements in the visible and the near-infrared regions, Applied Optics, 39, 2067-2070, 10.1364/ao.39.002067, 2000.

Osborne, S. R., Johnson, B. T., Haywood, J. M., Baran, A. J., Harrison, M. a. J. and 13McConnell, C. L.: Physical and optical properties of mineral dust aerosol during the 14Dust and Biomass−burning Experiment, J. Geophys. Res., 15113(D23), doi:10.1029/2007JD009551, 2008

https://doi.org/10.5194/ar-2026-20
Preprint. Discussion started: 11 June 2026

Perim de Faria, J., Bundke, U., Berg, M., Freedman, A., Onasch, T. B., and Petzold, A.: Airborne and laboratory studies of an IAGOS instrumentation package containing a modified CAPS particle extinction monitor, Aerosol Science and Technology, 51, 1240−1253, 10.1080/02786826.2017.1355547, 2017.

Petzold, A., Rasp, K., Weinzierl, B., Esselborn, M., Hamburger, T., Dörnbrack, A., Kandler, K., Schütz, L., Knippertz, P., Fiebig, M. and Virkkula, A.: Saharan dust absorption and refractive index from aircraft−based observations during SAMUM 2006, 26Tellus B, 61(1), 118–130, doi:10.1111/j.1600−0889.2008.00383.x, 2009.

Petzold, A., P. Formenti, D. Baumgardner, U. Bundke, H. Coe, J. Curtius, P. J. DeMott, R. C. Flagan, M. Fiebig, J. G. Hudson, J. McQuaid, A. Minikin, G. C. Roberts, and J. Wang, In Situ Measurements of Aerosol Particles, In: Manfred Wendisch and Jean−Louis Brenguier (eds); Airborne Measurements for Environmental Research: Methods and Instruments, First Edition, Wiley−VCH Verlag GmbH & Co, 2013.

Pinnick, R. G., J. D. Pendleton and G. Videen, Response Characteristics of the Particle Measuring Systems Active Scattering Aerosol Spectrometer Probes, Aerosol Science & Technology, 33:4, 334−352, DOI: 10.1080/02786820050121530, 2000.

Radney, J. G., and Zangmeister, C. D.: Comparing Aerosol Refractive Indices Retrieved from Full Distribution and Size− and Mass−Selected Measurements, J. Q. Spec. Rad. Trans., 220, 10.1016/j.jqsrt.2018.1008.1021, 10.1016/j.jqsrt.2018.08.021, 2018.

Reid, J. S., Kinney Reid, J. S. and Hobbs, P. V.: Physical and optical properties of young smoke from individual biomass fires in Brazil, J. Geophys. Res., 103, 32 013–32 030, 1998.

Reid, J. S., Westphal, D. L., Holben, B. N., Welton, E. J., Tsay, S.−C., Eleuterio, D. P., Campbell, J. R., Christopher, S. A., Colarco, P. R., Jonsson, H. H., Livingston, J. M., Maring, H. B., Meier, M. L., Pilewskie, P., Prospero, J. M., Reid, E. A., Remer, L. A., Russell, P. B., Savoie, D. L., Smirnov, A., and Tanré, D.: Analysis of measurements of Saharan dust by airborne and ground−based remote sensing methods during the Puerto Rico Dust Experiment (PRIDE), J. Geophys. Res., 108, 8586, doi:10.1029/2002JD002493, 2003.

Reddington, C. L., Carslaw, K. S., Stier, P., Schutgens, N., Coe, H., Liu, D., Allan, J., Browse, J., Pringle, K. J., Lee, L. A., Yoshioka, M., Johnson, J. S., Regayre, L. A., Spracklen, D. V., Mann, G. W., Clarke, A., Hermann, M., Henning, S., Wex, H., Kristensen, T. B., Leaitch, W. R., Pöschl, U., Rose, D., Andreae, M. O., Schmale, J., Kondo, Y., Oshima, N., Schwarz, J. P., Nenes, A., Anderson, B., Roberts, G. C., Snider, J. R., Leck, C., Quinn, P. K., Chi, X., Ding, A., Jimenez, J. L., & Zhang, Q. (2017). The Global Aerosol Synthesis and Science Project (GASSP): Measurements and Modeling to Reduce Uncertainty, Bull. Amer. Meteor. Soc., 98(9), 1857−1877.

Rosenberg, P. D., A. R. Dean, P. I. Williams, J. R. Dorsey, A. Minikin, M. A. Pickering, and A. Petzold (2012), Particle sizing calibration with refractive index correction for light scattering optical particle counters and impacts upon PCASP and CDP data collected during the Fennec campaign, Atmos. Meas. Tech., 5(5), 1147–1163, doi:10.5194/amt−5−1147−2012.

Ryder, C. L., Highwood, E. J., Rosenberg, P. D., Trembath, J., Brooke, J. K., Bart, M., Dean, A., Crosier, J., Dorsey, J., Brindley, H., Banks, J., Marsham, J. H., McQuaid, J. B., Sodemann, H., and Washington, R.: Optical properties of Saharan dust aerosol and contribution from the coarse mode as measured during the Fennec 2011 aircraft campaign, Atmos. Chem. Phys., 13, 303−325, doi:10.5194/acp−13−303−2013, 2013.

Schafer, J. S., Eck, T. F., Holben, B. N., Thornhill, K. L., Ziemba, L. D., Sawamura, P., Moore, R. H., Slutsker, I., Anderson, B. E., Sinyuk, A., Giles, D. M., Smirnov, A., Beyersdorf, A. J., and Winstead, E. L.: Intercomparison of aerosol volume size distributions derived from AERONET ground−based remote sensing and LARGE in situ aircraft profiles during the 2011–2014 DRAGON and DISCOVER−AQ experiments, Atmos. Meas. Tech., 12, 5289–5301, https://doi.org/10.5194/amt−12−5289−2019, 2019.

Seinfeld, J. H., and Pandis, S. N.: Atmospheric chemistry and physics: From air pollution to climate change, in, John Wiley and Sons, Inc., New York, 1326, 2nd edition, 2006.

Shettle, E. P., and Fenn, R. W.: Models for the aerosols of the lower atmosphere and the effects of humidity variations on their optical properties., Air Force Geophysics Laboratory, U.S. Air Force

https://doi.org/10.5194/ar-2026-20
Preprint. Discussion started: 11 June 2026

Geophysics Laboratory, Hanscomb Air Force Base, Mass., Environmental Research Papers 670 AFGL−TR−79−0214, 1979.

Shiraiwa, Manabu, Kayo Ueda, Andrea Pozzer, Gerhard Lammel, Christopher J. Kampf, Akihiro Fushimi, Shinichi Enami, Andrea M. Arangio, Janine Fröhlich−Nowoisky, Yuji Fujitani, Akiko Furuyama, Pascale S. J. Lakey, Jos Lelieveld, Kurt Lucas, Yu Morino, Ulrich Pöschl, Satoshi Takahama, Akinori Takami, Haijie Tong, Bettina Weber, Ayako Yoshino, and Kei Sato, Aerosol Health Effects from Molecular to Global Scales, Environmental Science & Technology 51 (23), 13545−13567, DOI: 10.1021/acs.est.7b04417, 2017

Szymanski, W. W., and Liu, B. Y. H.: On the Sizing Accuracy of Laser Optical Particle Counters, Particle & Particle Systems Characterization, 3, 1−7, https://doi.org/10.1002/ppsc.19860030102, 1986.

Szopa, S., V. Naik, B. Adhikary, P. Artaxo, T. Berntsen, W.D. Collins, S. Fuzzi, L. Gallardo, A. Kiendler-Scharr, Z. Klimont, H. Liao, N. Unger, and P. Zanis: Short-Lived Climate Forcers. In Climate Change 2021: The Physical Science Basis. Contribution of Working Group I to the Sixth Assessment Report of the Intergovernmental Panel on Climate Change [Masson-Delmotte, V., P. Zhai, A. Pirani, S.L. Connors, C. Péan, S. Berger, N. Caud, Y. Chen, L. Goldfarb, M.I. Gomis, M. Huang, K. Leitzell, E. Lonnoy, J.B.R. Matthews, T.K. Maycock, T. Waterfield, O. Yelekçi, R. Yu, and B. Zhou (eds.)]. Cambridge University Press, Cambridge, United Kingdom and New York, NY, USA, pp. 817–922, doi: 10.1017/9781009157896.008, 2021.

Velazco-Roa, M. A., and Thennadil, S. N.: Estimation of complex refractive index of polydisperse particulate systems from multiple-scattered ultraviolet-visible-near-infrared measurements, Applied Optics, 46, 3730-3735, 10.1364/ao.46.003730, 2007.

Walser, A., Sauer, D., Spanu, A., Gasteiger, J. and Weinzierl, B.: On the parametrization of optical particle counter response including instrument−induced broadening of size spectra and a self−consistent evaluation of calibration measurements, Atmospheric Measurement Techniques, 10(11), 4341–4361, doi:https://doi.org/10.5194/amt−10−4341−142017, 2017.

Weinzierl, B., Ansmann, A., Prospero, J., Althausen, D., Benker, N., Chouza, F., Dollner, M., Farrell, D., Fomba, W., Freudenthaler, V., Gasteiger, J., Gross, S., Haarig, M., Heinold, B., Kandler, K., Kristensen, T., Mayol−Bracero, O. L., Müller, T., Reitebuch, O., Sauer, D., Schäfler, A., Schepanski, K., Spanu, A., Tegen, I., Toledano, C., and Walser, A.: The Saharan Aerosol Long−Range Transport and AerosoŒ Cloud−Interaction Experiment: Overview and Selected Highlights, Bulletin of the American Meteorological Society, 98, 1427−1451, 2017.

Wendisch, M., and J.−L. Brenguier, Airborne Measurements for Environmental Research, Wiley−VCH., 2013.

Wu, H., Taylor, J. W., Szpek, K., Langridge, J. M., Williams, P. I., Flynn, M., Allan, J. D., Abel, S. J., Pitt, J., Cotterell, M. I., Fox, C., Davies, N. W., Haywood, J., and Coe, H.: Vertical variability of the properties of highly aged biomass burning aerosol transported over the southeast Atlantic during CLARIFY−2017, Atmos. Chem. Phys., 20, 12697–12719, https://doi.org/10.5194/acp−20−12697−2020, 2020.

Zieger, P., Väisänen, O., Corbin, J. C., Partridge, D. G., Bastelberger, S., Mousavi−Fard, M., Rosati, B., Gysel, M., Krieger, U. K., Leck, C., Nenes, A., Riipinen, I., Virtanen, A. and Salter, M. E.: Revising the hygroscopicity of inorganic sea salt particles, Nature Communications, 8, 15883, doi:10.1038/ncomms15883, 2017.